Article

Study of Influence of Boundary Condition of Diffuser with Non-Uniform Velocity on the Jet Characteristics and Indoor Flow Field

Kaijun Li [ID]**, Linye Song, Xinghui Zhang *** [ID]**, Qi Wang and Jing Hua**

School of Civil Engineering, Taiyuan University of Technology, Taiyuan 030024, China
*   Correspondence: zxhtut@163.com

Abstract: In practice, the outflow from a diffuser is highly non-uniform due to many reasons. However, the air outflow velocity from a diffuser is uniform in most current studies. Little research has been conducted to determine under what conditions uniform velocity can be used. Therefore, based on the non-uniformity of velocity, airflow characteristics of grille and ceiling diffusers were investigated experimentally and numerically. Two generic CFD cases (non-uniform and uniform velocity) are presented. The velocity field near the diffuser is investigated with measurements in order to determine velocity-inlet boundary conditions. The study shows that the uniform velocity-inlet boundary condition can be considered accurate only under certain conditions. For the grille diffuser, the aspect ratio affects the distribution of the outflow velocity. Using uniform velocity as the velocity-inlet boundary condition for the grille diffuser would result in at least a 14.2% error in the jet region, except when the outflow aspect ratio is 1 and the average velocity is greater than 1.83 m/s. However, when the average velocity of the ceiling diffuser is 3.64 m/s, the error of using uniform velocity as the velocity-inlet boundary condition reaches 58.3%. This study provides the basis for determining the velocity-inlet boundary conditions during numerical simulations.

Keywords: non-uniform velocity; boundary condition; CFD; diffuser; air supply opening

1. Introduction

With the development of computers, the application of Computational Fluid Dynamics (CFD) technology has been popularized. Many scholars regard numerical simulation as a significant tool for indoor air quality and the assessment of ventilation systems [1,2]. The main task of any ventilation and air-conditioning system in rooms is to guarantee thermal comfort for the occupants and provide a suitable preservation environment [3]. Many aspects determine the satisfaction of occupants concerning the ambient conditions, including air velocity [4], asymmetries of temperature distribution in the room [5], and thermal radiation of surfaces [6]. The first two factors are directly related to the ventilation system used and the diffusers used. The selection, location, number, and types of supply diffusers are essential to achieve suitable air quality and optimal thermal conditions in the ventilated space [7]. According to the American Society of Heating Refrigerating and Air-Conditioning Engineers (ASHRAE), assuming that the occupied area is inhabited anywhere, the velocities in the occupied zone should remain below 0.25 m/s [8]. In general, the occupied zone is defined as the volume of the room between the elevation of the floor and 1.8 m above the floor [9]. In ventilation system design, 0.2 m/s is usually regarded as a limit value [9].

Air is usually supplied to a room through diffusers located on the ceiling, floor, or wall. The way that air is distributed to the room is closely related to the structure of the supply diffuser. There have been many studies using numerical calculations and experimental analysis on the air distribution of diffusers [10,11]. When CFD is used to simulate room air flow, the air supply opening boundary conditions have a great influence on indoor air

flow [12,13]. The direct description of the diffuser is a natural idea [14,15]. However, it requires millions of grid cells, resulting in a large amount of calculation and even non-convergence. Proper specification of diffuser boundary conditions is the essential element in accurate prediction of the air distribution in a ventilated room [16]. Several simplified methods for diffusers have been proposed.

In the box method, all boundary conditions are measured data for each diffuser and thus limit its use [17,18]. The method of how to determine the box size has been given [19]. However, the box method is not suitable for low-Reynolds-number flows, such as floor-level air supply systems [20]. The prescribed velocity method reduces the number of measurements required compared to the box method, and the measured data were specified at some crucial positions [17,18]. The main region specification method makes full use of the velocity and temperature attenuation formulas of the main jet section and avoids the measurement of each parameter [21]. However, this method depends on the accuracy of the diffuser characteristic jet equation [22].

In the basic model, the diffuser is modeled by a simple opening with the same effective area as the diffuser, which should have the same aspect ratio as the real diffuser [23,24]. The model predicted good airflow patterns in isothermal indoor environments [25]. However, the model behaved poorly for small non-isothermal flow [24], uniform velocity magnitudes, velocity direction [26], and effective flow area [27,28].

An improvement to this basic model is the momentum method [29]. The diffuser is replaced with a simple opening with the same area, and the boundary conditions of the continuity equation and the momentum equations are set separately. The merge of the small jets is accompanied with momentum loss [30]. The loss of momentum flux for a single jet is less than the loss for many individual jets with the same total area as the single jet. Hence, the momentum is not conserved.

An improvement to this momentum method is the total-flux momentum method, which explains that the momentum method is not applicable for a fine grid adjacent to the diffuser from the viewpoint of discretization, and which is presented to include both the convective flux and the diffusion flux in the momentum source [31]. Another improvement to the momentum method is the superficial density method, which keeps the inlet mass flow and momentum flux consistent with the actual values by changing the inlet air density [25].

In the N-point air supply opening model (ASMO), the effective area coefficient for calculating the inlet momentum source term in the CFD code is used [32]. However, most CFD software does not support the definition of the coefficient of the effective area at the inlet. In the inlet cell blocking method, the mass and momentum boundary conditions were satisfied by using the random mathematical function to determine if a CFD cell is open [22]. It was thought to be better for diffusers with a large supply area. However, it needs to be implemented by user-defined functions (UDFs) and cannot be simply used.

Much research has been done to simplify the modeling of the diffuser, but these methods still have many shortcomings. Previous CFD studies of various models ignored the inhomogeneity of the actual diffuser velocity and only considered the diffuser velocity as an even velocity based on the fully open area [33]. It is well known that the outflow from the diffuser is non-uniform because the nature of the air flow is turbulent and depends on the characteristics of the diffuser. Abdelmaksoud [34] found that a tile located in the RL data center shows highly non-uniform velocity distribution over these pores. For an ideal (uniform) flow velocity that has the same flow rate as the non-uniform flow velocity, the flow momentum of the latter will always be greater because momentum scales with velocity squared. When resulting in non-uniform and complex velocity distributions, none of these diffuser modeling methods seem to be useful for detailed predictions of airflow and temperature distributions [26]. Iyengar et al. [35] concluded that either the use of a single opening with reduced flow area or the use of a body force field may not predict the rapid rise in tile flow. Abdelmaksoud [34] concludes that defining different velocities through multiple holes can effectively reduce errors, which is a great improvement to the full open tile model.

In order to address the aforementioned issues, this study proposes a simplified method based on non-uniform velocity. The calculation method based on the experiment and CFD simulation is introduced. The effects of uniform and non-uniform velocity as boundary conditions on the jet characteristics and the interior flow field, respectively, are investigated to illustrate the potential reasons for refining the boundary conditions in CFD simulations.

2. Concept and Calculation Method of Non-Uniform Velocity

2.1. Definition of Non-Uniform Velocity

In this study, the non-uniform outflow velocity is based on the time-independent assumption. The magnitude of the velocity from the diffuser depends only on the location of the outflow from the diffuser. For example, at the edge of the diffuser, the magnitude of the outflow velocity is small. At the center of the diffuser, the magnitude of the outflow velocity is large. The direction of the outflow velocity depends only on the angle of the different blades of the diffuser. The outflow velocity is no longer considered as a uniform value. The meanings of 'non-uniform' mentioned in this paper are based on this definition.

2.2. Calculation Method of Non-Uniform Velocity

Since velocity is the main parameter in the indoor flow field, obtaining the velocity distribution at the diffuser through experimental measurements is the first step towards an accurate evaluation. Figure 1 shows the technical route of this study. First, the velocity distribution at the outlet of the three diffusers under different exit conditions was obtained by experimental measurements. After analyzing the experimental results, the velocity-inlet boundary conditions were provided for further numerical calculations. The accuracy of the model was verified by comparing the experimental data with the numerical simulation results. It provides a basis for further analysis of the effects of different boundary conditions on the jet characteristics and numerical simulation results of the indoor flow field.
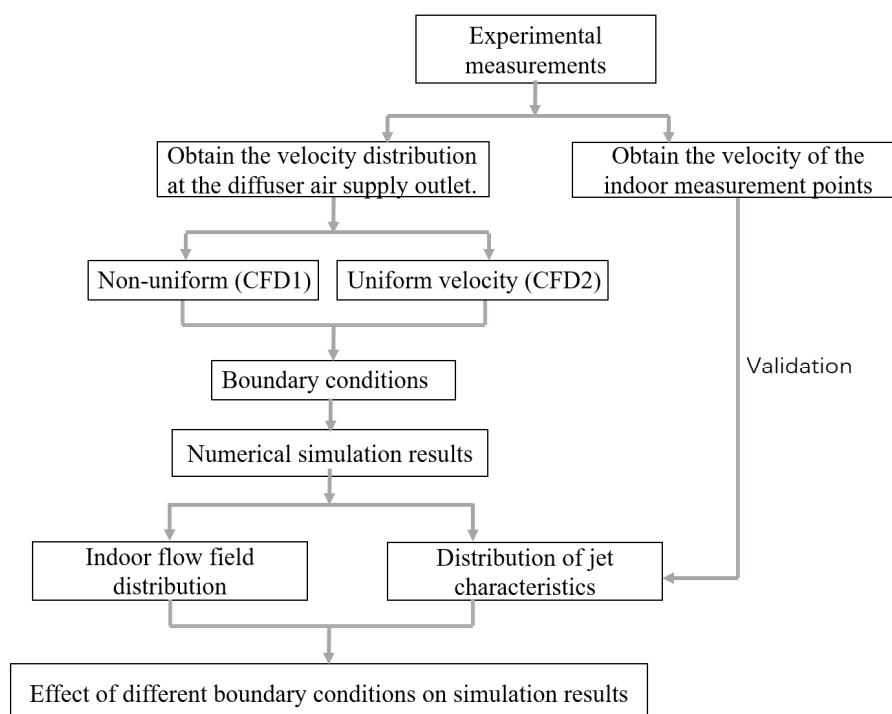

Figure 1. Technical route of study.

3. Experimental Work

3.1. Experimental Setup

The general layout of the experimental setup is shown in Figure 2. It is mainly composed of two parts: an air-conditioning unit and airflow chamber (model room). Air is

supplied by a fan equipped with a frequency converter. The flow rate is controlled by a frequency converter transducer, which can be adjusted steplessly. The airflow enters the room from the upper plenum chamber in which the tested diffuser is installed. The room consists of a confined space with dimensions of 10.9 m (length) × 4.9 m (wide) × 2.9 m (high). The data acquisition system DAQ970A is also shown in Figure 2. The DAQ970A can measure temperature, ac/dc volts, resistance, frequency, or current. The DAQ970A has read rates of over 5000 readings per second and scan rates of up to 450 channels per second in a single channel. Therefore, the system can meet the needs of experimental data acquisition. Figure 3 shows three types of supply air diffusers used in the experiments. The dimensions of the square grille diffuser (SGD) and square ceiling diffuser (SCD) are 300 mm × 300 mm, as shown in Figure 3a,c. The dimensions of the rectangle grille diffuser (RGD) is 440 mm × 220 mm, as shown in Figure 3b. The effective area coefficients calculated from the measured results are 0.64 (SGD), 0.68 (RGD), and 0.87 (SCD). The SGD and SCD are installed on the ceiling of the room. The RGD is installed on the upper part of the side wall. The air velocity of the diffuser and indoor area are measured by hot-wire anemometer. Table 1 shows the specification and range of the experimental measurement instrument.

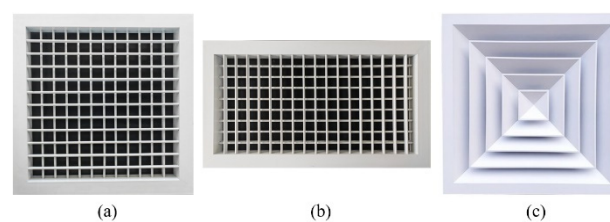**Figure 2.** Layout of the experimental setup.

Figure 3. Types of supply air diffusers. (**a**) SGD; (**b**) RGD; (**c**) SCD.

Table 1. Specification and range of velocity-measuring instrument.

Model	Range	Accuracy	Resolution
CTV114	0~2 m/s	$\pm3\%$ of reading ±0.05 m/s	0.01 m/s
CTV115	0~15 m/s	$\pm3\%$ of reading ±0.2 m/s	0.1 m/s

3.2. Experimental Procedure

In the present work, three types of diffusers are studied. The velocity of the air supply opening can be changed by adjusting the frequency of the converter. Each diffuser is installed and investigated sequentially. The range of the studied inlet air velocity is shown in Tables 2 and 3. The velocity sensor is attached to the bracket, and its height can be adjusted up and down. When measuring air velocity in the vertical direction, the plumb line is used to determine that the measuring point is on the same straight line. When measuring the horizontal direction, the vertical distance of the instrument from the diffuser is determined first. Then, the fixed bracket cannot move up and down. The airflow velocity at different locations is measured by moving the whole bracket horizontally. Similarly, to ensure that the horizontal measuring points are in the same straight line, a line is fixed horizontally at the same height as the sensor probe. The line diameter used in the experiments is 0.26 mm, which would not affect the experimental results. The data transmission interval was set as 3 s, and each measuring point was measured for 3 min. The system is allowed time to stabilize after each velocity adjustment. In order to ensure the accuracy of the experimental measurement, these procedures are repeated more than 3 times with an interval of more than 3 h.

Table 2. Flow boundary conditions for different grille diffusers.

Case			CFD1				CFD2	
Diffuser		**SGD**		**RGD**			**SGD**	**RGD**
Zone		**M1**	**M2**	**M1**	**M2**	**M3**	**N1**	**N1**
	15 Hz	1.92	1.53	1.84	2.04	1.38	1.83	1.85
Velocity (m/s)	10 Hz	1.25	0.98	1.42	1.58	0.77	1.19	1.08
	5 Hz	0.56	0.45	0.67	0.71	0.42	0.54	0.47

Table 3. Flow boundary conditions for square ceiling diffuser.

Case				CFD1			CFD2
Zone		**M1**	**M2**	**M3**	**M4**		**N1 ~ N4**
	25 Hz	4.48	4.4	2.78	1.5		3.64
	20 Hz	3.55	3.31	2.82	1.63		3.03
Velocity (m/s)	15 Hz	2.71	2.5	1.74	1.02		2.18
	10 Hz	1.62	1.45	1.3	0.58		1.34
	5 Hz	0.82	0.62	0.62	0.33		0.65

Figure 4 shows the distribution of measurement points in the diffuser. In this paper, it is assumed that the outlet velocity distribution from the diffusers is symmetric. The distribution of measurement points of the indoor air jet is shown in Figure 5. For the SGD, Pole 1 is located on the SGD axis (as shown in Figure 5a). The first measuring point is 10 cm away from the SGD. One measuring point is arranged every 10 cm from measuring point 1 to 11. One measuring point is arranged every 20 cm from measuring point 11 to 17. The last measuring point is 0.5 m away from the ground. To obtain the cross-sectional velocity distribution of SGD, the measurement points located on lines Z_1 to Z_3 are tested separately. The interval between the two measuring points is 5 cm. The distance of the

last measuring point from Pole 1 is 45 cm. For the RGD, Pole 2 is located on the RGD axis (as shown in Figure 5b). Pole 3 and Pole 4 are 10 cm and 30 cm away from Pole 2, respectively, and on the same horizontal plane. The area between Pole 2 and Pole 4 has the same distribution of measurement points. The first measuring point is 10 cm away from the SGD. One measuring point is arranged every 5 cm from measuring point 1 to 7. One measuring point is arranged every 10 cm from measuring point 7 to 19. To obtain the cross-sectional velocity distribution of the RGD, the measurement points located on lines X_1 to X_3 are tested separately. The interval between the two measuring points is 5 cm. The range from X_1 to X_3 has 11, 11, and 13 measuring points, respectively. For the SCD, 11 measuring points are arranged every 0.3 m along the jet direction (as shown in Figure 5a).
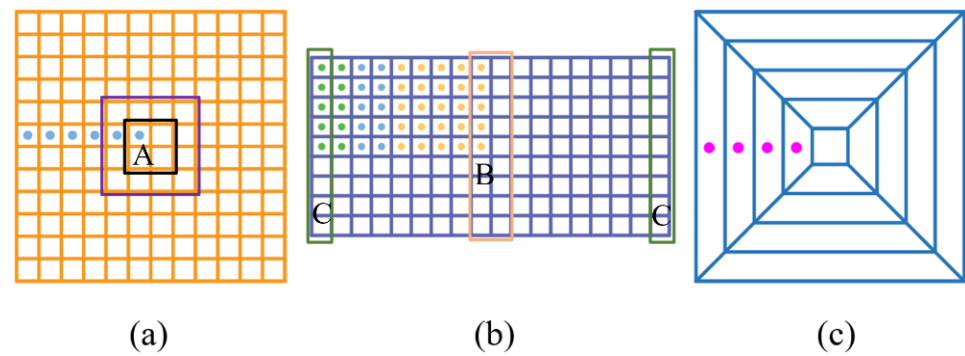

Figure 4. Distribution of measuring points in tuyere. (**a**) SGD; (**b**) RGD; (**c**) SCD. (A, B, and C represent the area circled in the box).
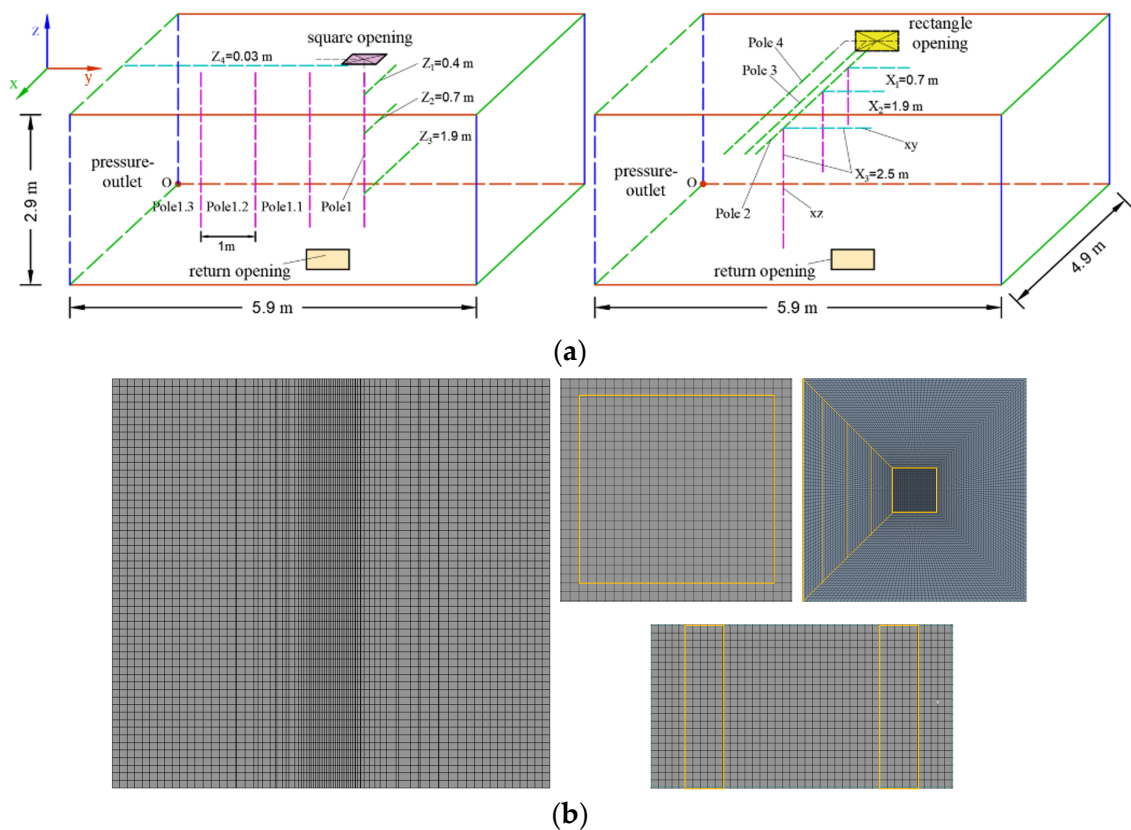

Figure 5. The computational physical model and mesh. (**a**) Layout of the physical model; (**b**) the computational mesh.

4. Numerical Model

The room under consideration had the following dimensions: a length by width by height of 5.9 m × 4.9 m × 2.9 m (see Figure 5a). By comparing the full-scale experimental model with the present study model (Figure 5a), the results show that the error between the two is less than 2%. Hence, only half of the airflow room is taken for simulation in order to reduce the amount of calculation. The pressure outlet is taken from the left wall of the model. The air was supplied through the grille and ceiling diffusers, which are located as shown in Figure 5. The return opening is at the lower part of the side wall, which is located 0.1 m above the floor. The computational domain is discretized into hexahedral grids. The average mesh quality of the models is above 0.85, which can be considered reliable for the simulation results. The growth rate factor was set as 1.2. The view of the computational mesh used is shown in Figure 5b.

The flow in the indoor environment can be described by the continuity equation, the momentum equation, and the turbulence model. The commercial software ANSYS Fluent is used to solve the governing equations. All equations can be described by the following equation:

$$\frac{\partial \rho \Phi}{\partial t} + \frac{\partial \rho u_j \Phi}{\partial x_j} = \frac{\partial}{\partial x_j}\left(\Gamma_{eff}\frac{\partial \Phi}{\partial x_j}\right) + S_\Phi \tag{1}$$

where Φ is the solved variable, which can be 1, u, v, w, k, or ε, u_j is the velocity component, x_j is the coordinate, Γ_{eff} is the effective diffusion coefficient. When $\Phi = 1$, Equation (1) becomes the continuity equation.

Several structured grids are performed with different mesh sizes for each diffuser to guarantee the grid independence of the results. This paper compares the velocity at 1.9 m of the diffuser axis at 69.1 K, 89.4 K, 129.5 K, 229.4 K, 288.2 K, 395.5 K, and 628.5 K grid quantity. The result shows that 229.4 K grid size can be considered to be grid independence, with a maximum percentage error of about 1.55% compared to the mesh size of 628.5 K.

RNG k-ε models can then be used to deal with global comfort prediction as well as thermal ventilation efficiency in isothermal terms [36]. Therefore, the RNG k-ε model is used to describe the turbulence. To model the flow near the wall, standard wall functions are used. For discretization, all flow variables are in second-order format, and the pressure–velocity coupling algorithm is SIMPLE. The computation is assumed convergent when all residuals are less than 1.0×10^{-4}.

No-slip boundary conditions are used along the room walls, the ceiling, and the floor ($V_x = V_y = V_z = 0$). In the present study, the air jet is an isothermal jet. All walls, ceiling, and floor are assumed to be adiabatic walls ($q = 0$). Values of the inlet boundary conditions are evaluated through experimental measurements. Furthermore, for turbulent flows, turbulence intensity and hydraulic diameter are set at the inlet section. For all cases, 20% turbulence intensity is used, and the hydraulic diameter is calculated by Equation (2). Numerical values of the velocity-inlet boundary conditions used for the solution are listed in Tables 2 and 3. The data in the table are calculated from the experimental results, and the calculation procedure is detailed later.

$$D_e = 4 \times \frac{A_c}{\chi} \tag{2}$$

where D_e is the hydraulic diameter, A_c is cross-sectional flow area, χ is the wetted perimeter.

5. Results and Discussion

5.1. Determination of Final Inlet Boundary Conditions

Taking the velocity of the diffuser at 15 Hz as an example, the origin was used to draw the cloud map according to the experimental measurement data, as shown in Figure 6. In fact, the velocity distribution characteristics of the diffuser are independent of the fan speed, as shown in Figure 7. From this figure, it is clear that the velocity distribution is non-uniform. The outflow from the diffuser is non-uniform because the nature of the air

flow is turbulent and depends on the characteristics of the diffuser. The wall shear stress around the non-circular duct is not uniformly distributed. Due to the effect of shear force on the wall of the duct, the distribution of air flow velocity in the duct section is not uniform. The structure of the diffuser itself enhances the non-uniformity of the air outlet surface. Therefore, it is necessary to consider the non-uniformity of outflow velocity. The simple openings should be divided according to outflow direction and velocity distribution as shown in Figure 8. It can also be seen from Figure 6b that there is no significant difference in the velocity magnitude of RGD in the width direction. When the aspect ratio of the grid diffuser is greater than 2, the velocity distribution in the width direction can be considered uniform. The conclusion was further verified using measured data for different sizes with the same aspect ratio, which is still correct.
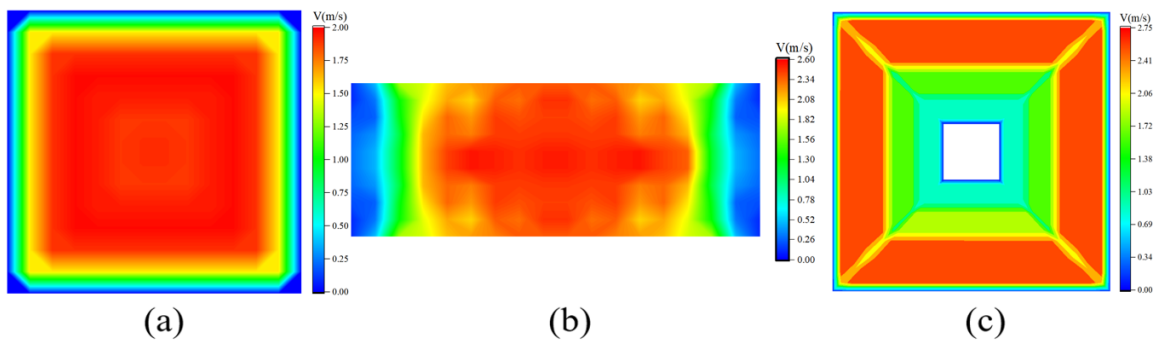

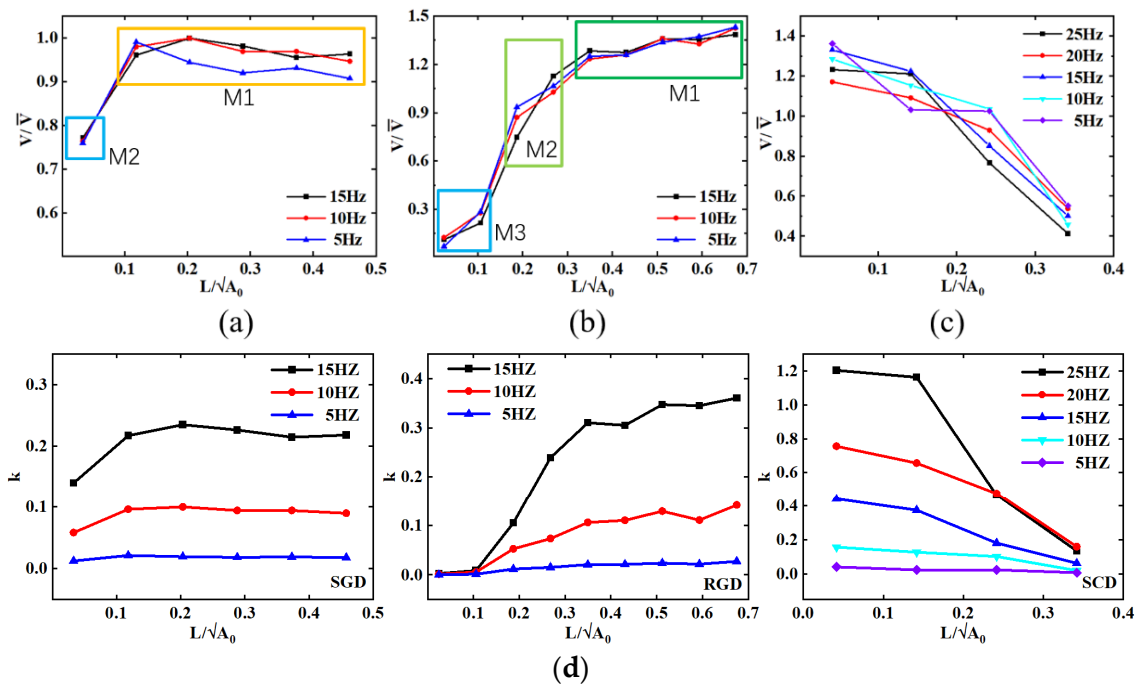**Figure 6.** Velocity contours of measured results at 15 Hz. (**a**) SGD; (**b**) RGD; (**c**) SCD.

Figure 7. Dimensionless velocity and k plot distribution of measured results. (**a**) SGD; (**b**) RGD; (**c**) SCD; (**d**) k plots across the chosen diffuser plane.
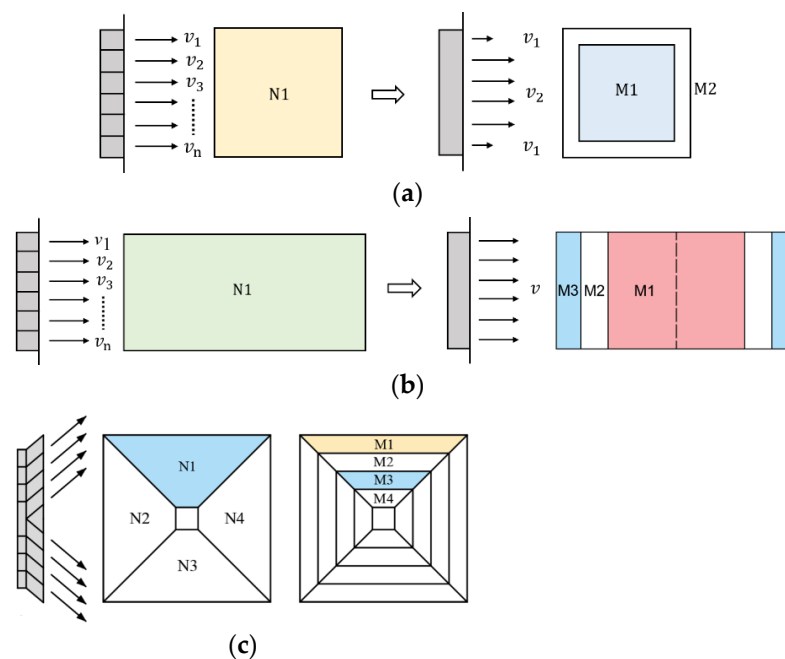
Figure 8. Diffuser velocity-inlet area division. Uniform velocity-inlet case on the left, non-uniform velocity-inlet case on the right. (**a**) Square grille diffuser. (**b**) Rectangle grille diffuser. (**c**) Square ceiling diffuser.

Figure 7 shows the distributions of the dimensionless velocity ($V/\overline{V}$) and dimensionless distance ($L/\sqrt{A_0}$) at the diffuser. The average velocity can be calculated as follows:

$$\overline{V} = \frac{\sum_{i=1}^{m} V_i A_i}{A} \tag{3}$$

where V_i is the velocity of the measuring point and A_i is the area of the region represented by the measurement point. For example, the velocity of a point in region A represents the velocity magnitude of the whole region in Figure 4a. For the RGD, the velocity is considered to be unchanged in the width direction. Hence, the average velocity of measuring points in area B is first calculated. The average velocity represents the velocity distribution in the orange box region in Figure 4b. The calculation results are shown in Tables 2 and 3 (N1~N4). The turbulent kinetic energy k increases with the increase in outflow velocity, as shown in Figure 7d. This non-uniformity distribution can have an impact on thermal comfort. Since k has the same trend as the velocity variation, both boundary conditions are classified in the same way.

Based on the velocity dimensionless magnitude and the magnitude of the slope between two points, the following relevant conclusions can be obtained. It is clear that the SGD and SCD have a similar trend under different conditions. For the SGD, the velocity in the M2 region is significantly smaller than the overall flow rate. The velocity variation in the M1 region is small (slope of about 0.5). When establishing the air supply outlet boundary conditions, the velocity magnitude in the M1 region can be considered as a constant. Therefore, the air outlet boundary conditions for the SGD can be simplified to M1 and M2 in the numerical simulation, as shown in Figures 7a and 8a. The distribution of the RGD is more complex compared to the SGD. It has been assumed that the velocity magnitude does not change with the width direction. As can be seen in Figure 7b, the RGD has an additional transition region compared to the SGD. Therefore, the air outlet boundary conditions for the SGD can be simplified to M1, M2, and M3 in the numerical simulation, as shown in Figures 7b and 8b. However, for the SCD, the velocity distribution monotonically decreases from the edge of the diffuser to the center of the diffuser. Therefore,

the air outlet boundary conditions of the SCD cannot be further simplified, as shown in Figures 7c and 8c.

From the above analysis, it can clearly be concluded that the outflow from the diffuser is non-uniform. The measured data are then used to further analyze the effects of uniform and non-uniform velocities as boundary conditions on the jet characteristics and indoor flow field.

In order to better define the non-uniform velocity under inflow boundary conditions, CFD1 and CFD2 will be used in this study to represent the two cases of non-uniform and uniform velocity, respectively. Figure 8 shows the two modeling approaches for the three diffusers. N is the number of outlet flow directions. M is determined on the basis of N based on the velocity distribution, as shown in Figure 8. For the SCD, the velocity distribution is not as obvious as that of grille diffusers, as shown in Figure 7c. In order to consider the impact of velocity non-uniformity, a detailed simulation analysis of the SCD is carried out, as shown in Figure 8c.

For grille diffusers, the velocity in M_i area is the average velocity of measuring points in M_i area (shown in Figure 5). The average velocity can be calculated as follows:

$$V_{M_i} = \frac{\sum_{i=1}^{n} V_i}{n} \tag{4}$$

where V_i is the velocity of the measuring point and V_{Mi} is the average velocity of the measuring point in M_i area.

For the ceiling diffuser, the velocity in M_i area is the velocity of measuring points in M_i area.

The calculation results are shown in Tables 2 and 3.

5.2. Effect of Two Types of Boundary Conditions on Jet Characteristics

Figure 9 shows the comparison between experimental and numerical data of velocity decay for the square grille diffuser under different outflow conditions. From this figure, it is clear that the simulation results of the CFD1 agree well with the experimental data. The axial velocity decay and cross-sectional velocity decay of CFD1 and experiment measurements are smaller than those of CFD2. It is shown that the real jet characteristics can be accurately simulated when the velocity distribution at the air supply outlet is considered to be non-uniform. When the velocity is high ($\overline{V} = 1.83$), the maximum error of velocity distributions is less than 5% at Pole 1, and it can be concluded that the two types of boundary conditions have little effect on the simulation results. However, when the velocity is small ($\overline{V} = 0.54$), the velocity non-uniformity has a great influence on the simulation results, and the maximum error of velocity distributions is 14.2%. This may be the reason why some previous models failed to describe low-Reynolds-number flows. Hence, for a diffuser with a low flow rate, non-uniform velocity as a boundary condition is recommended to improve the calculation accuracy of jet characteristics.

Figure 10 presents the calculated and measured velocity distributions of the rectangle grille diffuser. In order to highlight the jet characteristics of the RGD, the dimensionless velocity (V_m / V_{max}) and dimensionless distance ($X / \sqrt{A_0}$) are adopted. From Figure 10, it can be seen that the RGD is more strongly influenced by the non-uniform velocity-inlet boundary conditions compared to SGD. The axial velocity decay and cross-sectional velocity decay of CFD1 and the experiment measurements are faster than those of CFD2. The uniform velocity-inlet boundary condition is not sufficient to simulate the jet characteristics of RGD. That is, the real jet characteristics can be accurately simulated when the velocity distribution at the air supply outlet is considered to be non-uniform. Hence, for a diffuser with a large aspect ratio, the effect of velocity non-uniformity of outflow should be considered. The same trend is observed in the cross-sectional plane of the jet main region, which is consistent with the Gaussian error function formula. At low velocity ($\overline{V} = 0.47$), although the overall trend is consistent, individual points differ greatly. This may be due to

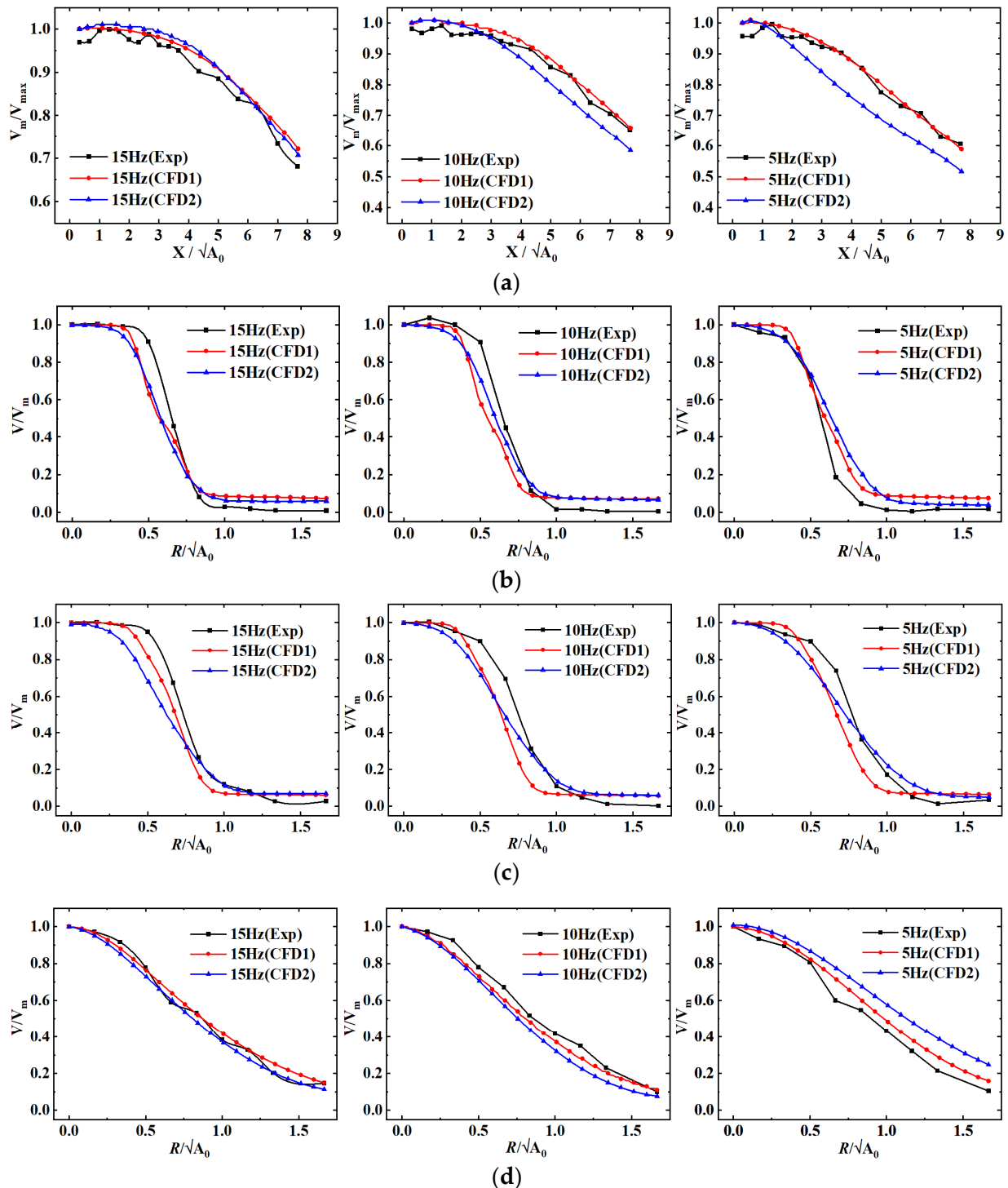the high instability of the airflow and the error caused by the instrument in measuring the low velocity.

Figure 9. Comparison of measured and numerical profiles for SGD at four positions. (**a**) Pole 1. (**b**) Z_1. (**c**) Z_2. (**d**) Z_3.

As can be seen in Figures 9 and 10, the rectangular jet with a larger aspect ratio forms a strong vortex structure at the exit, which leads to a rapid decay of the central velocity. As the aspect ratio increases, the fluctuation velocity and turbulence of the jet increase significantly after the exit, reflecting the significant increase in the ability of the surrounding fluid to be sucked [37]. Compared with the uniform velocity boundary condition, the axial

velocity decay of the non-uniform velocity boundary condition is significantly influenced by the aspect ratio.

For the square ceiling diffuser, the supply air spreads in all directions so it is more complicated than the two grilles above. Figure 11 shows the distributions of the dimensionless velocity (V/V_{max}) and dimensionless distance ($X/\sqrt{A_0}$) at the Z_4. According to the outlet characteristic, N is set to four as shown in Figure 8c. The calculated velocity of the ceiling diffuser matches well with the measured data of CFD1. As can be seen from Figure 11, when the outflow average velocity is 3.64 m/s (25Hz), CFD2 will cause a large numerical error. The maximum error of velocity distributions is 58.3%, which is unacceptable. When uniform velocity is used as the velocity-inlet boundary condition, the axial jet decay curve of SCD cannot be realistically simulated. Therefore, for ceiling diffusers, the non-uniformity of the outflow velocity should be considered.
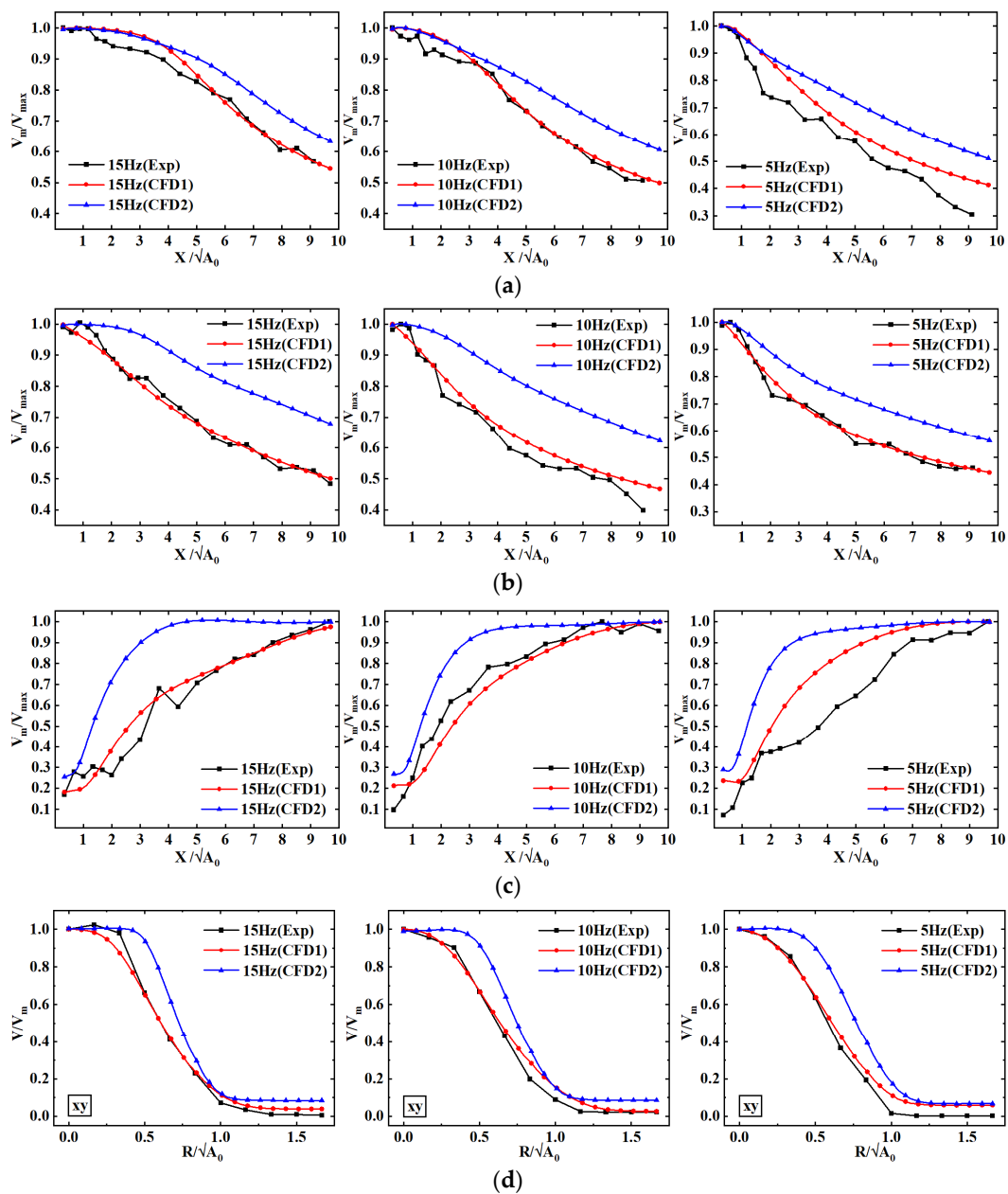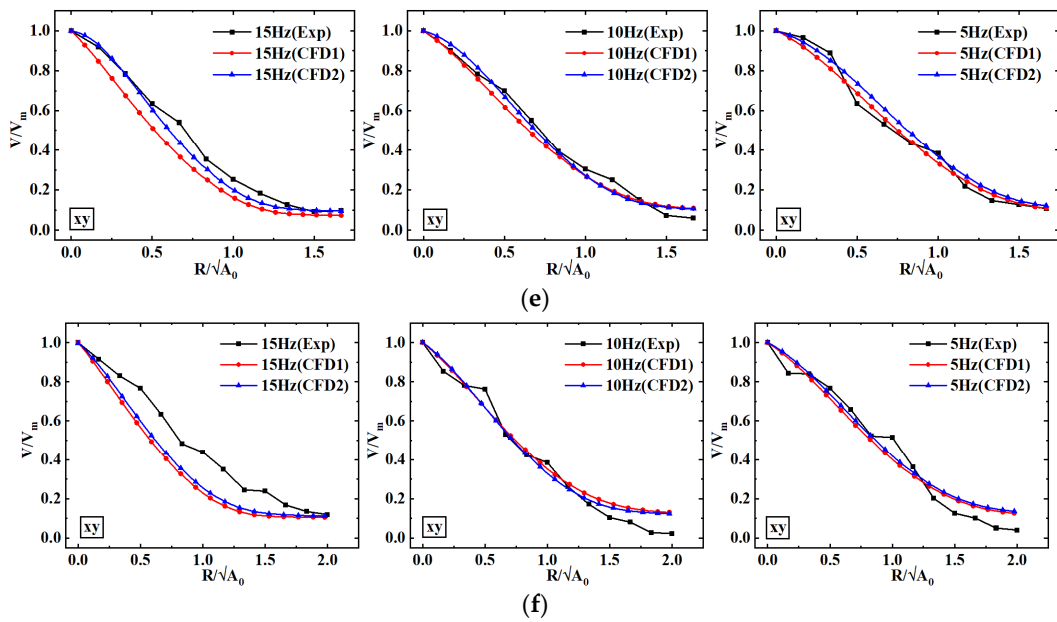

Figure 10. *Cont.*

Figure 10. Comparison of measured and numerical profiles for RGD at nine positions. (**a**) Pole 2. (**b**) Pole 3. (**c**) Pole 4. (**d**) X_1. (**e**) X_2. (**f**) X_3.
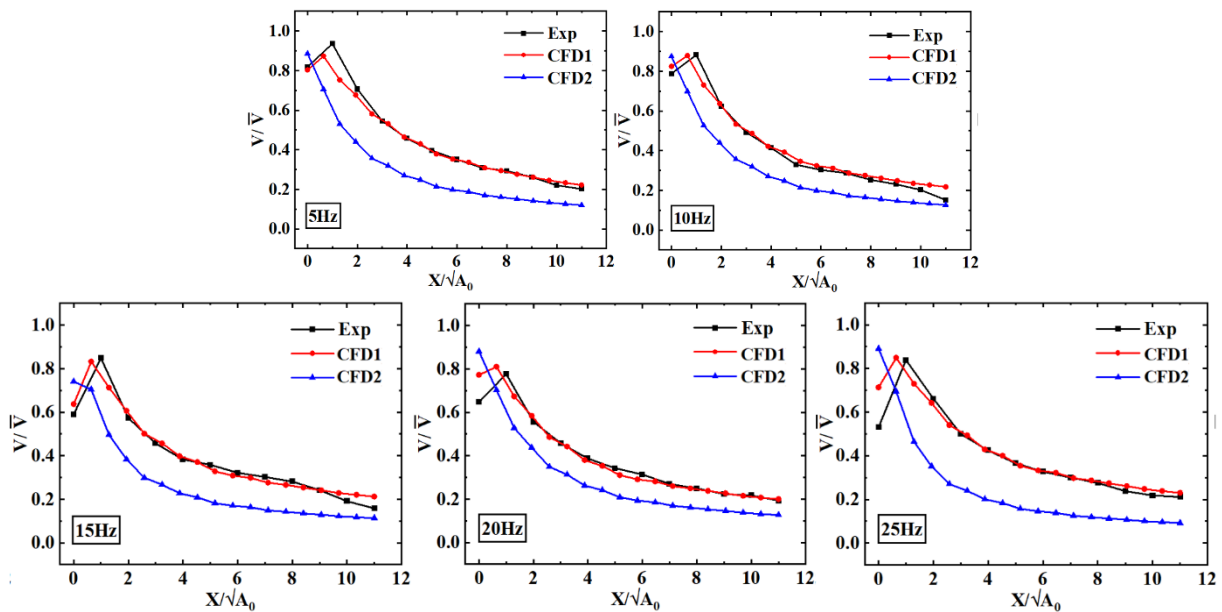

Figure 11. Comparison of measured and numerical profiles for SCD at Z_4.

5.3. Effect of Two Types of Boundary Conditions on Indoor Flow Field

By comparing the simulated and experimental values of the jet characteristic curves, it can be concluded that the model is able to accurately simulate the actual situation. Next, the effects of the two types of boundary conditions on the indoor flow field are further analyzed.

Figure 12 shows the numerical data of indoor velocity profiles under different outflow conditions. It is clear that the outflow velocity distribution has a significant influence on the indoor flow field. When the velocity is high ($\overline{V} = 1.83$), the maximum error of the velocity distribution in the occupation zone is 19.5% within 1 m from the diffuser jet area. The difference between the two can be ignored outside the 2 m range of the jet area. However, when the velocity is small ($\overline{V} = 0.54$), the two types of boundary conditions have almost no effect on the overall indoor flow field.
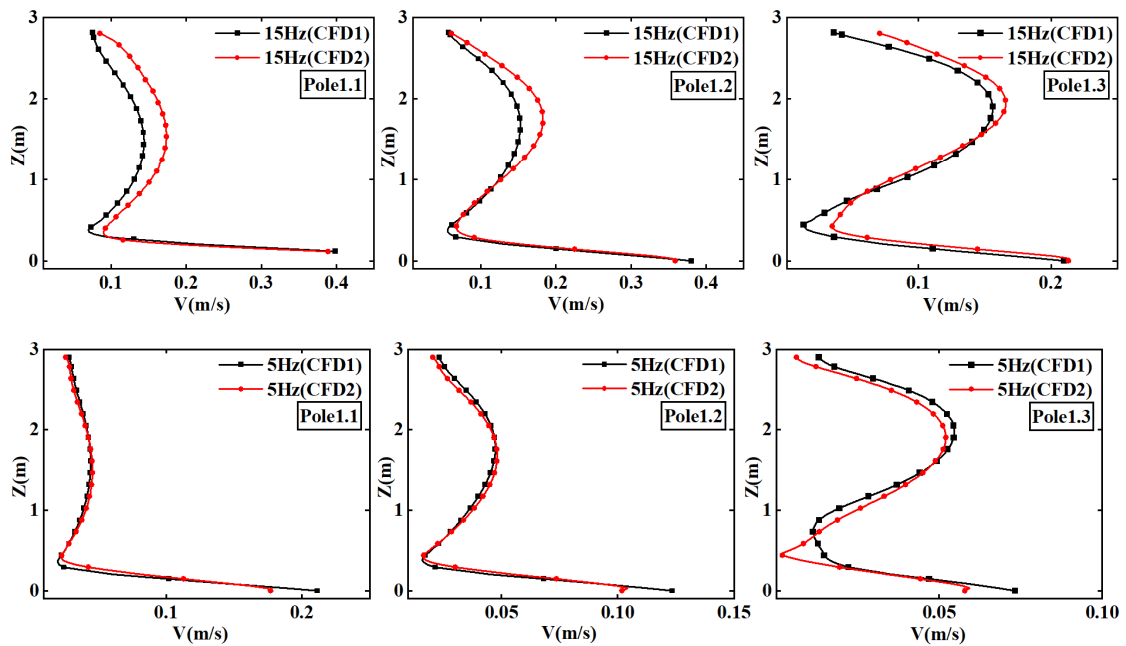
Figure 12. Calculated velocity profiles for SGD at three positions.

Figure 13 shows the numerical data of velocity profiles for RGD under different outflow conditions. Similar to SGD, when the outflow velocity is small ($\overline{V} = 0.47$), the two types of boundary conditions have no effect on the indoor flow field. The same conclusion can be drawn when evaluating the effect of velocity on human comfort. When the velocity is high ($\overline{V} = 1.85$), the maximum error of CFD2 indoor velocity distributions in the occupied zone (X_1-xz) is 21.6%. However, the velocity in the occupied area is less than 0.2 m/s beyond the 1 m range of the jet zone. This is related to the fact that RGD is an air-conditioning form with upper side air supply and uniform velocity in the width direction.
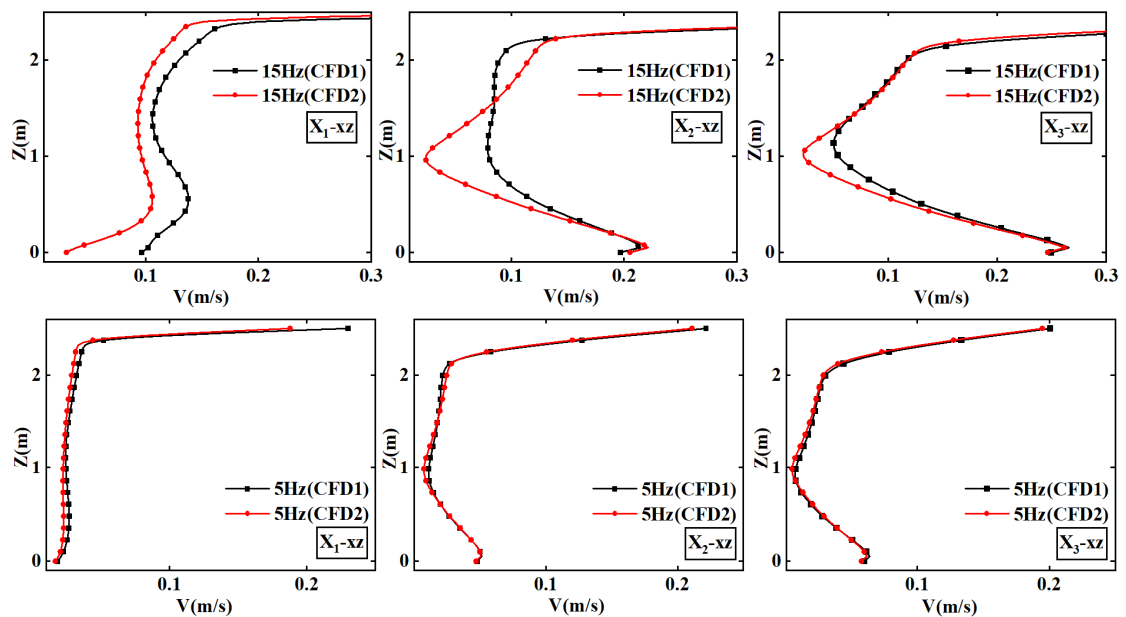

Figure 13. Calculated velocity profiles for RGD at three positions.

Figure 14 shows the numerical data of velocity profiles for SCD under different outflow conditions. In contrast to SGD and RGD, when the velocity is small ($\overline{V} = 3.64$), the two types of boundary conditions have a significant effect on the jet section. The wall-adherent jet

performance of the SCD is obviously reduced. This may be due to the increased inertial forces and gravitational effects. When the velocity inlet is less than the average velocity of 1.34 m/s, the two types of boundary conditions have almost no effect on the jet section.
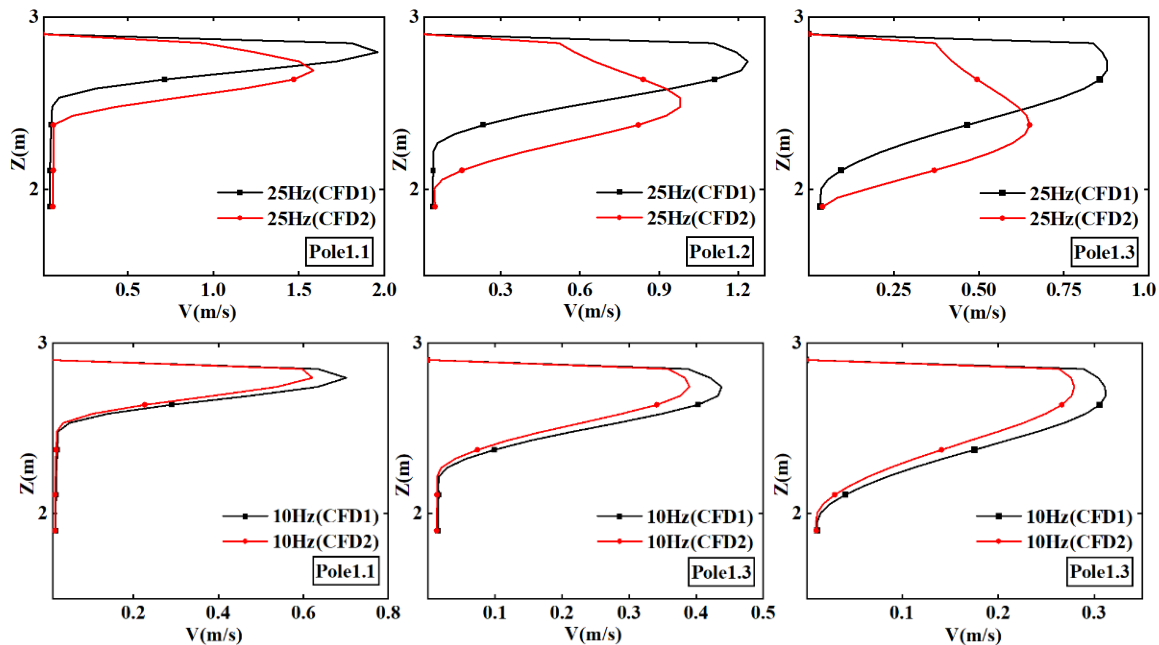

Figure 14. Calculated velocity profiles for SCD at three positions.

For SCD, when the average velocity is 3.64 m/s, the error of using uniform velocity as the velocity-inlet boundary condition reaches 58.3%. The simulation results of uniform velocity as velocity-inlet boundary condition in the jet region can be considered accurate when the average outflow velocity is below 1.34 m/s, as shown Figure 14. For SGD and RGD, the error of the indoor velocity field increases with the increase in the air outflow velocity. When the average velocity is about 1.8 m/s, the maximum error of the velocity distribution in the occupation area is about 20%. However, for the ceiling diffuser, it can be seen that the affected area is within 0.3–1.0 m from the height of the diffuser.

6. Conclusions

The non-uniform velocity and uniform velocity-inlet boundary conditions are determined by experimental measurements. The effects of non-uniform velocity and uniform velocity as boundary conditions on the jet characteristics and indoor flow field were investigated, respectively. The following conclusions can be drawn from this study.

1. For grid diffusers, the aspect ratio affects the distribution of the outflow velocity from the diffuser. When the aspect ratio of the grid diffuser is greater than 2, the velocity distribution in the width direction can be considered uniform. For ceiling diffusers, the velocity distribution monotonically decreases from the edge of the diffuser to the center of the diffuser.

2. When the aspect ratio is 1 and the average outflow velocity exceeds 1.83 m/s, the effect of the non-uniformity of the outflow velocity of the grid diffuser on the jet characteristics does not exceed 5%. Furthermore, the use of uniform velocity as the velocity-inlet boundary condition will result in at least a 14.2% error. Because underfloor air supply usually sends air directly into the room at low air velocity, it is particularly important to consider the uniformity of the outflow velocity.

3. When the average air velocity of the air supply outlet is greater than 2.0 m/s, the error brought by the non-uniform outflow velocity to the indoor flow field must be considered.

Nomenclature

A	Area (m^2)
A_0	Gross area of the diffuser (m^2)
L	Distance from the edge of the diffuser (m)
R	Radial distance of the point from the centerline of the jet (m)
RGD	Rectangle grille diffuser
SCD	Square ceiling diffuser
SGD	Square grille diffuser
S_Φ	Source term
V$_m$	Centerline velocity (m/s)
X	Distance from diffuser (m)
Γ_{eff}	Effective diffusion coefficient
m	Mass flow rates (kg/s)
k	Turbulent kinetic energy
q	Heat flux (W/m^2)
t	Time
x, y, z	Co-ordinate system
ρ	Air density (kg/m^3)
Subscripts	
in	Simple opening inlet conditions
r	Real conditions
max	Maximum

References

1. Zhu, H.-C.; Cao, S.-J. Fast prediction for multi-parameters (concentration, temperature and humidity) of indoor environment towards the online control of HVAC system. In *Building Simulation*; Tsinghua University Press: Beijing, China, 2020; Volume 14.
2. Yau, Y.; Poh, K.; Badarudin, A. A numerical airflow pattern study of a floor swirl diffuser for UFAD system. *Energy Build.* **2018**, *158*, 525–535. [CrossRef]
3. Dang, Y.; Luo, X.; Chang, B.; Huang, X.; Feng, Z.; Gu, Z. Local attachment ventilation system for the unearthed relic preservation area within site museum. *Sustain. Cities Soc.* **2022**, *77*, 103537. [CrossRef]
4. *ISO 7730:2005*; Ergonomics of the Thermal Environment—Analytical Determination and Interpretation of Thermal Comfort Using Calculation of the PMV and PPD Indices and Local Thermal Comfort Criteria. International Organization for Standardization: Geneva, Switzerland, 2006.
5. *ANSI/ASHRAE Standard 55-2004*; Thermal Environmental Conditions for Human Occupancy. American Society of Heating, Refrigerating and Air-Conditioning Engineers, Inc.: Atlanta, GA, USA, 2004.
6. Alfano, F.R.A.; Olesen, B.W.; Palella, B.I.; Riccio, G. Thermal comfort: Design and assessment for energy saving. *Energy Build.* **2014**, *81*, 326–336. [CrossRef]
7. Varodompun, N. HVAC Ventilation Strategies: The Contribution for Thermal Comfort, Energy Efficiency, and Indoor Air Quality. *J. Green Build.* **2007**, *2*, 131–150. [CrossRef]
8. American Society of Heating Refrigerating and Air-Conditioning Engineers, Inc. *ASHRAE Handbook—Heating, Ventilating, and Air-Conditioning Applications*, SI ed.; American Society of Heating Refrigerating and Air-Conditioning Engineers, Inc.: Washington, DC, USA, 2015.
9. Halibart, J.; Zwolińska, K.; Borowski, M.; Jaszczur, M. Analysis of the Velocity Distribution in the Plenum Box with Various Entries. *Energies* **2021**, *14*, 3630. [CrossRef]
10. Li, A.; Yang, C.; Tong, R.; Bao, X.; Qin, E.; Gao, R. PIV experiment and evaluation of air flow performance of swirl diffuser mounted on the floor. *Energy Build.* **2017**, *156*, 58–69. [CrossRef]

11. Hurnik, M.; Kaczmarczyk, J.; Popiolek, Z. Study of Radial Wall Jets from Ceiling Diffusers at Variable Air Volume. *Energies* **2021**, *14*, 240. [CrossRef]
12. Jun, L. *Research and Application of Air Supply Opening Models in CFD Simulation*; Southwest Jiaotong University: Chengdu, China, 2012.
13. Nielsen, P. Description of Supply Openings in Numerical Models for Room Air Distribution. *Ashre Trans. Symp.* **1991**, *98*, 26.
14. Hu, S.C. Airflow characteristics in the outlet region of a vortex room air diffuser. *Build. Environ.* **2003**, *38*, 553–561. [CrossRef]
15. Topp, C.; Jensen, R.L.; Pedersen, D.N.; Nielsen, P.V. Validation of Boundary Conditions for CFD Simulations on Ventilated Rooms. In Proceedings of the 4th International Conference on Indoor Air Quality, Ventilation & Energy Conservation in Buildings, iAQVEC 2001, Changsha, China, 2–5 October 2001.
16. Huo, Y.; Haghighat, F.; Zhang, J.S.; Shaw, C.Y. A systematic approach to describe the air terminal device in CFD simulation for room air distribution analysis. *Build. Environ.* **2000**, *35*, 563–576. [CrossRef]
17. Nielsen, P.V.; Restivo, A.; Whitelaw, J.H. The velocitycharacteristics of ventilated rooms. *Trans ASME J. Fluids Eng.* **1978**, *100*, 291–298. [CrossRef]
18. Gosman, A.D.; Nielsen, P.V.; Restivo, A.; Whitelaw, J.H. The Flow Properties of Rooms with Small Ventilation Openings. *Trans. Asme* **1980**, *102*, 316–323. [CrossRef]
19. Srebric, J.; Chen, D.Q. A Method of Test to Obtain Diffuser Data for CFD Modeling of Room Airflow (RP1009). *ASHRAE Trans.* **2001**, *107*, 108–116.
20. Xu, H.T.; Niu, J.L. A new method of CFD simulation of airflow characteristics of swirling floor diffusers. *Proc Build. Simul.* **2003**, *3*, 1429–1434.
21. Huo, Y.; Zhang, J.S.; Shaw, C.Y.; Haghighat, F. A New method to describe the diffuser boundary conditions in CFD simulation. *Indoor Air* **1996**, *96*, 233–240.
22. Zhang, T.; Lee, K.; Chen, Q. A simplified approach to describe complex diffusers in displacement ventilation for CFD simulations. *Indoor Air* **2009**, *19*, 255–267. [CrossRef]
23. Heikkinen, J. Modelling of a supply air terminal for room air flow simulation. In Proceedings of the Air Movement &Ventilation Control within Buildings, Ottawa, ON, Canada, 24–27 September 1991.
24. Chen, Q.; Moser, A. Simulation of a multiple-nozzle diffuser. In Proceedings of the 12th ATVC Conference on Air Movement and Ventilation Control within Buildings, The TEA AirInfiltration and Ventilation Centre, Ottawa, ON, Canada, 24–27 September 1991; Volume 2, pp. 1–13.
25. Deng, B.; Zhang, Y.; Long, F. A superficial density method to describe the diffuser boundary condition in CFD simulation of indoor airflow. *Build. Environ.* **2018**, *135*, 280–285. [CrossRef]
26. Cehlin, M.; Moshfegh, B. Numerical modeling of a complex diffuser in a room with displacement ventilation. *Build. Environ.* **2010**, *45*, 2240–2252. [CrossRef]
27. Skovgaard, M. Turbulent Flow in Rooms Ventilated by Mixing Principle: Comparision between Computational Fluid Dynamics and Full-Scale Experiments. Ph.D. Thesis, Department of Building Technology and Structural Engineering, Aalborg University, Aalborg, Denmark, 1991. *Indoor Environmental Technology* Vol. R9145 No.
28. Emvin, P.; Davidson, L. Numerical comparison of three inlet approximations of the diffuser in case E1 Annex20. In Proceedings of the 5th International Conference on Air Distributions in Rooms ROOMVENT '96, Yokohama, Japan, 17–19 July 1996; Volume 1, pp. 219–226.
29. Chen, Q.; Suter, P.; Moser, A. Influence of air supply parameters on indoor air diffusion. *Build. Environ.* **1991**, *26*, 417–431. [CrossRef]
30. Lai, J.C.S.; Nasr, A. Two parallel plane jets: Comparison of the performance of three turbulence models. *Proc. Inst. Mech. Eng. Part G J. Aerosp. Eng.* **2005**, *212*, 379–391. [CrossRef]
31. Deng, B.; Wang, J.; Tang, J.; Gao, J. Improvement of the momentum method as the diffuser boundary condition in CFD simulation of indoor airflow: Discretization viewpoint. *Build. Environ.* **2018**, *141*, 55–60. [CrossRef]
32. Zhao, B.; Li, X.; Yan, Q. A simplified system for indoor airflow simulation. *Build. Environ.* **2003**, *38*, 543–552. [CrossRef]
33. Abdelmaksoud, W.A. Simplified CFD Model for Perforated Tile with Distorted Outflow. *Fluids* **2022**, *7*, 112. [CrossRef]
34. Abdelmaksoud, W.A. Experimental and Numerical Investigations of the Thermal Environment in Air-Cooled Data Centers. Ph.D. Thesis, Department of Mechanical and Aerospace Engineering, Syracuse University, Syracuse, NY, USA, 2012.
35. Iyengar, M.; Schmidt, R.R.; Hamann, H.; VanGilder, J. Comparison between Numerical and Experimental Temperature Distributions in a Small Data Center Test Cell. In Proceedings of the ASME 2007 InterPACK Conference, Vancouver, BC, Canada, 8–12 July 2007; pp. 819–826.
36. Kuznik, F.; Rusaoueen, G.; Brau, J. Experimental and numerical study of a full scale ventilated enclosure: Comparison of four two equations closure turbulence models. *Build. Environ.* **2007**, *42*, 1043–1053. [CrossRef]
37. Ma, Z.; Xu, M.; Luan, J.; Liu, X.; Zhao, F. Statistical properties of turbulent free jets issuing from rectangular nozzles with different aspect ratios. *J. Exp. Fluid Mech.* **2017**, *31*, 54–61.